PFilter: Building Persistent Maps through Feature Filtering for Fast and Accurate LiDAR-based SLAM

Yifan Duan, Jie Peng, Yu Zhang, Jianmin Ji* and Yanyong Zhang

Abstract— Simultaneous localization and mapping (SLAM) based on laser sensors has been widely adopted by mobile robots and autonomous vehicles. These SLAM systems are required to support accurate localization with limited computational resources. In particular, point cloud registration, i.e., the process of matching and aligning multiple LiDAR scans collected at multiple locations in a global coordinate framework, has been deemed as the bottleneck step in SLAM. In this paper, we propose a feature filtering algorithm, *PFilter*, that can filter out invalid features and can thus greatly alleviate this bottleneck. Meanwhile, the overall registration accuracy is also improved due to the carefully curated feature points.

We integrate *PFilter* into the well-established scan-to-map LiDAR odometry framework, F-LOAM, and evaluate its performance on the KITTI dataset. The experimental results show that *PFilter* can remove about 48.4% of the points in the local feature map and reduce feature points in scan by 19.3% on average, which save 20.9% processing time per frame. In the mean time, we improve the accuracy by 9.4%.

I. INTRODUCTION

Simultaneous localization and mapping (SLAM) plays a vital role in navigation of autonomous systems like autonomous carscite and robots [1]. In recent years, with the development of LiDAR technology [2], LiDAR-based SLAM has attracted a great deal of attention because of LiDAR's capabilities of remaining robust against illumination changes and obtaining accurate distance information [3]. In fact, LiDAR-based SLAM is often used to estimate the robot's ego-motion, denoted as LiDAR odometry (LO), and locate itself in the map, denoted as localization [4]. In this paper, we consider how to improve the efficiency and accuracy of LO through better feature selection.

Point cloud registration, i.e., the process of matching and aligning multiple LiDAR scans collected at multiple locations in a global coordinate framework, has been deemed as a major time-consuming task in LO. It is usually modeled as a nonlinear least-squares problem on suitable feature points, and solved by optimization methods like Gauss-Newton or Levenberg-Marquardt. Due to the large number of points in a LiDAR frame – for example, a 64-line LiDAR has about 120 thousand points per frame – typical registration methods such as ICP [5] and NDT [6] usually involve a large amount of computations (e.g., nearest neighbor queries, gradient descent-based optimizations, etc.) with a risk of non-convergence [7]. The other disadvantage stems from their

* The corresponding author.

School of Computer Science and Technology, University of Science and Technology of China, Hefei, 230026, China {dyf0202, pengjieb}@mail.ustc.edu.cn, {yuzhang, jianmin, yanyongz}@ustc.edu.cn.

(a) Local edge map before *PFilter* (b) Local edge map after *PFilter*

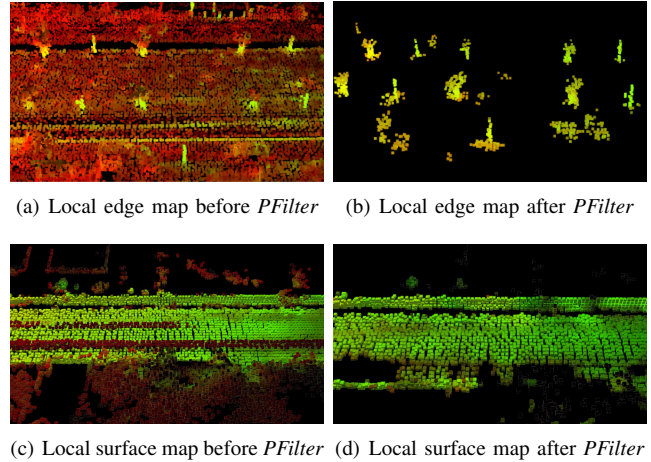(c) Local surface map before *PFilter* (d) Local surface map after *PFilter*

Fig. 1. The effect of *PFilter* for a local feature map consisting of a local edge map and a local surface map. Each point in the maps is colored by its p-Index value: the red color indicates points with low p-Index values, i.e., transient feature points, while the green color indicates points with high p-Index values, i.e., persistent feature points. The local maps (a) and (c) contain a large number of incorrectly extracted features; after filtering out these erroneous feature points, the resulting maps in (b) and (d) contain fewer feature points that should be included for registration. Here, the edge map in (b) only keeps landmarks such as poles, trunks, while the surface map in (d) only keeps landmarks such as ground and walls.

sensitivity to initial poses, which can severely undermine the subsequent correspondence establishment process.

To address the two issues, a popular approach [8] is to extract features from the raw data according to the geometric properties, and only use a portion of the point cloud for registration. Even with such downsampling operations, the point cloud registration still remains the bottleneck for many state-of-the-art SLAM systems [9], [10], severely limiting the efficiency of the whole SLAM system.

Several schemes have been proposed to address this bottleneck through clever feature selection. For example, the schemes discussed in [11]–[14] try to reduce the number of constraints for registration by adding new geometric conditions or by evaluating the contribution or uncertainty of constraints to the optimization equation. While these schemes have explored the distribution of feature points in each individual point cloud frame, the distribution of feature points across consecutive frames are largely unexplored.

In this paper, we set out to explore the cross-frame feature point distribution for more efficient feature selection. Towards this end, we propose a new attribute for feature points, named persistence-index, p-Index in short. p-Index evaluates whether a feature point is *persistent* or *transient* by observing its distribution across consecutive frames, which is weighed by how frequent a feature point is detected recently.

Intuitively, larger p-Index values are assigned to those feature points that have been detected frequently in the near past. We call feature points with large values of p-Index as persistent.

In our experiments, we find out that, feature points that are persistent usually correspond to stationary landmarks, like lamp poles, tree trunks, grounds, walls, etc. On the contrary, transient feature points are usually generated occasionally, possibly due to events such as occlusion, moving objects or even software bugs. Including these transient feature points in registration not only increases the amount of computation that is required, but also makes the algorithm more prone to errors. As such, our main idea is to filter out these transient feature points, and retain the persistent ones as much as possible. The filtering algorithm using p-Index is called *PFilter*.

In our implementation, we integrate *PFilter* into the scan-to-map LO framework. We keep only persistent features in the local feature map, while filtering out transient ones after a period of observation. *PFilter* can not only greatly reduce the feature point count in the local map as showed in Fig. 1, but also considerably reduce the constraints in the registration process. In the evaluation, we test two popular feature extraction algorithms with *PFilter*, and both prove that our algorithm can improve both the efficiency and the accuracy of LO.

In summary, our main contributions are as follows:

- We propose a new attribute p-Index to evaluate feature points, which indicates whether a point is persistent or transient. Our *PFilter* algorithm carefully curates the suitable feature points by filtering out the transient ones;
- We integrate *PFilter* into the scan-to-map LO system, and conduct experiments on KITTI dataset [15] to demonstrate that *PFilter* can improve the efficiency and accuracy at the same time. The experimental results show that *PFilter* can remove about 48.4% of the points in the local feature map and reduce feature points in scan by 19.3% on average, which save 20.9% time per frame on average and improves the accuracy by 9.4%.

II. RELATED WORK

A. LiDAR Odometry

LO has boomed in recent years. Since LOAM [8] in 2015, there have been various variants, like F-LOAM [9], LeGO-LOAM [16], LiLi-OM [17], LOAM-Livox [18], based on its framework. In particular, LeGO-LOAM [16] segments ground points and splits the optimization into two step to reduce search space. F-LOAM [9] abandons the scan-to-scan match and replaces it by only scan-to-map with high frequency. Mulls [10] breaks down the types of features further and optimize the registration algorithm. LiLi-OM [17] and LOAM-Livox [18] extent LOAM to solid-state LiDAR.

B. Feature Selection

Feature selection considers how to extract subsets from raw data while maintaining the accuracy. ROI-cloud [19] presents a key region extraction method. Aiming at removing dynamic and redundant point cloud, they voxelize 3D space into weighted cubes, and update the "importance" of each cubes continuously. Jiao et al. [11] use stochastic-greedy algorithm to select good features according to motion information on the premise of preserving the spectral property of information matrices. Inspired by the Dilution Of Precision (DOP) concept in the field of satellite positioning, KFS-LIO [12] proposes a quantitative evaluation method for constraints derived from features and integrates the method in tightly-coupled LiDAR inertial odometry framework. Faster-GICP [14] incorporates acceptance-rejection sampling-based two-step point filter into the GICP method. Wan et al. [13] formulate the uncertainty model, sensitivity model, and contribution theory to calculate the contribution of every residual term. With the idea similar to feature selection, Yin et al. [20] scores the points in map by observation count for map compression and Pomerleau, François et al. [21] computes whether a point is dynamic or static based on multiple observations.

As a similar work, ROI-cloud [19] also updates status of points across consecutive frames. However, ROI-cloud uses geometric information to evaluate the importance of each cube, while we use p-Index to evaluate *persistence* level of a feature point.

C. Semantic SLAM

Using semantic information to understand the scene is also a way to extract persistent features. Dong et al. [22] extract poles from point cloud to realize reliable and accurate localization. VI-Eye [23] exploits traffic domain knowledge by detecting a set of key semantic objects including road, lane lines. They extract a small number of salience points and leverage them to achieve accurate registration of two point clouds. This method achieves amazing experimental results, but relies heavily on semantic segmentation and spends the most time on it. In this paper, we intent to provide an approach to automatically extract the most informative regions by observing the historical registration process to achieve similar results without the help of semantic information.

III. PRELIMINARIES

Before presenting *PFilter*, we first review the formulation of the point cloud registration problem. Then, we introduce two methods to extract feature points which are widely used in LO. It has shown that these feature extraction methods can improve the efficiency and the robustness of the registration process.

A. Formulation of Registration

As specified in [7], given two point clouds $\mathcal{P}_0$, $\mathcal{P}_1$ and their poses $\mathcal{X}_0$ and $\mathcal{X}_1$ in the same coordinate, the goal of registration is to estimate the transformation $\mathbf{T}^*$ from $\mathcal{X}_0$ to $\mathcal{X}_1$. In the point-to-point ICP algorithm [5], $\mathbf{T}^*$ can be calculated by:

$$\mathbf{T}^* = \arg\min_{\mathbf{T}} \quad \|d(\mathcal{P}_0, \mathbf{T}(\mathcal{P}_1))\|^2 \qquad (1)$$

where $d(\cdot, \cdot)$ denotes the loss function to measure the distance, and $\mathbf{T} = \begin{bmatrix} \mathbf{R} & \mathbf{t} \\ \mathbf{0} & 1 \end{bmatrix}$, where $\mathbf{R} \in SO(3)$ is the rotation matrix and $\mathbf{t} \in \mathbb{R}^3$ is the translation vector.

B. Feature Extraction

To reduce the number of considered points in ICP, feature extraction focuses on the local geometric structures of the point cloud. We review two of such methods that have been widely applied in LO.

The first feature extraction method applied in LOAM [8], LeGO-LOAM [16], and F-LOAM [9], utilizes the unique format of point clouds of mechanical LiDAR. This method is also considered as the feature extraction method based on "ring". The kth frame $\mathcal{L}_k$ from LiDAR is composed of several parallel rings consists of points continuously. We denote $\mathbf{p}_k^{(m,n)}$ for the nth point on the mth ring in the kth frame point cloud, then the smoothness $c_k^{(m,i)}$ of $\mathbf{p}_k^{(m,i)}$ is calculated by the neighborhood of $\mathbf{p}_k^{(m,i)}$ on the same ring. More details can be found in [8], [9], [16]. By setting some thresholds, two special types of points can be extracted from $\mathcal{L}_k$, called edge features, denoted as $\mathcal{E}_k$, and surface features, denoted as $\mathcal{S}_k$.

The second method applied in Mulls [10] and LiLi-OM [17], is not limited to the special structure, i.e., the ring, of the point cloud from LiDAR. This method is also considered as the feature extraction method based on eigenvalues. $\mathcal{L}_k$ is first stored in the KD-tree, and then the points denoted as $\mathcal{N}_k^i$ in the neighborhood of $\mathbf{p}_k^i$ can be found in $O(\log n)$. $\mathcal{N}_k^i$ can be the nearest m points or the points within a sphere of radius r. By calculating the eigenvalues $\lambda_1 > \lambda_2 > \lambda_3$ of the covariance matrix of $\mathcal{N}_k^i$, we can also define two variables to describe the local roughness of the point cloud. Linearity θ_l and planarity θ_p are defined as $\theta_l = \frac{\lambda_1 - \lambda_2}{\lambda_1}$ and $\theta_p = \frac{\lambda_2 - \lambda_3}{\lambda_1}$. Similarly, by setting some thresholds, the edge features and the surface features can be extracted from L_k.

With the edge features and the surface features, the loss function $d(\cdot, \cdot)$ in Eq. (1) can be replaced by the distance between edge features and edge extracted previously and the distance between surface features and surface as follows:

$$d_e(\mathbf{p}_e, \mathbf{p}_e^M, \mathbf{n}_e^M) = \|(\mathbf{T}\,\mathbf{p}_e - \mathbf{p}_e^M) \times \mathbf{n}_e^M\|, \\ d_s(\mathbf{p}_s, \mathbf{p}_s^M, \mathbf{n}_s^M) = (\mathbf{T}\,\mathbf{p}_s - \mathbf{p}_s^M) \cdot \mathbf{n}_s^M, \quad (2)$$

where $\mathbf{p}_e$, $\mathbf{p}_s$ are the edge and surface features, $\mathbf{p}_e^M$, $\mathbf{p}_s^M$ are the geometric center of the corresponding edge and the corresponding surface and $\mathbf{n}_e^M, \mathbf{n}_s^M$ are the unit vector of the edge and the norm of the surface.

The two methods have different standards for the filtering of points and resulting different sets of extracted features. In our experiments, we also evaluate the performance of *PFilter* based on these different sets of extracted features, respectively. More details will be specified in Sec. V-D.

IV. METHODOLOGY

In this section, we first give the overview of our system. Then we present the de-skewing and rough filtering in the
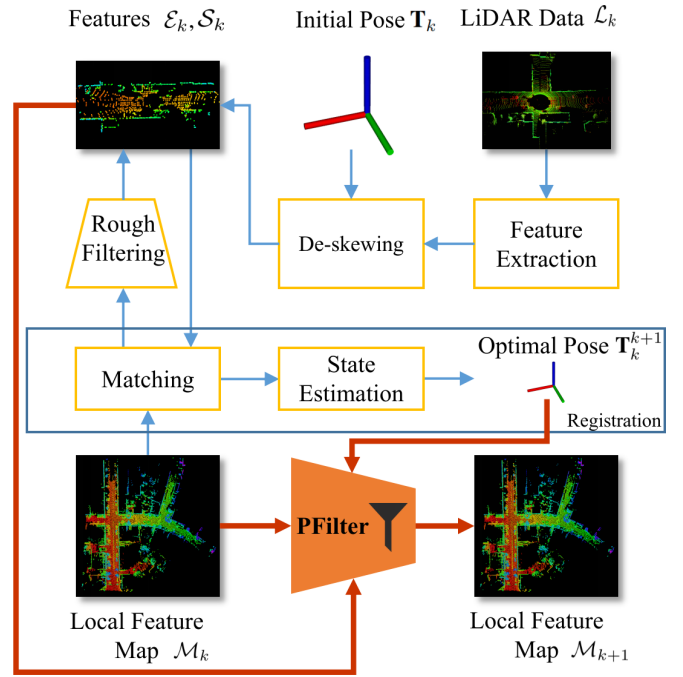

Fig. 2. Pipeline of the scan-to-map LO with *PFilter*. The red arrows indicate the input and output of *PFilter*.

system. Finally, we discuss the definition of p-Index and specify the details of *PFilter*.

A. Overview

As shown in [24], [25], scan-to-map registration is generally more robust than scan-to-scan registration as the latter accumulates error faster. Then we use the scan-to-map LO (LiDAR odometry) system, F-LOAM [9], as the base for our discussion and evaluation. The two sources of registration in Eq. (1) are feature points extracted from the scan and the local feature map, respectively.

As shown in the pipeline in Fig. 2, for the kth frame, the input of the LO system consists of the three parts, i.e., a local feature map, denoted as $\mathcal{M}_k = \{\mathbf{p}_0^M, \mathbf{p}_1^M, \ldots \mathbf{p}_n^M\}$, a frame of point cloud generated by LiDAR (i.e., 'LiDAR data' in the figure), denoted as $\mathcal{L}_k$, and an initial pose, denoted as $\mathbf{T}_k$. In particular, a local feature map $\mathcal{M}_k$ consists of two parts, i.e., $\mathcal{M}_k = \mathcal{M}_k^e \cup \mathcal{M}_k^s$, where $\mathcal{M}_k^e$ denotes the set of edge feature points and $\mathcal{M}_k^s$ denotes the set of surface feature points. At the beginning, we apply the feature extraction method as discussed in Sec. III-B on $\mathcal{L}_k$, which results in two sets of feature points, i.e., edge features, $\mathcal{E}_k$, and surface features, $\mathcal{S}_k$. Later, these extracted features are further processed to reduce motion distortion, e.g., through de-skewing and rough filtering that will be detailed in Sec. IV-B. During registration, each point in the local feature map updates its p-Index which measures the point's persistence level according to the match process, and will be definited in Sec. IV-C. At the end, the local feature map will be filtered by *PFilter* according to the resulting features and the optimal pose to remove transient features. The details of *PFilter* will be introduced in Sec. IV-D.

B. De-skewing and rough filtering

To handle motion distortion, we assume that the LiDAR maintains the same motion in two adjacent frames, which is generally valid due to the high frequency of LiDAR (typically 10Hz). In specific, the distortion is corrected by applying a constant angular velocity and a linear velocity to predict the motion between two consecutive LiDAR scans, which generates better initial pose of each feature point for registration.

After assigning these initial poses for feature points, we apply rough filtering to remove incorrect matches between such a feature point and its corresponding points in the local feature map. The rough filtering is similar to the method used in LOAM [8], which utilizes the distances between the feature point and its corresponding points, calculated by Eq. (2) and the geometric property of the corresponding points. After rough filtering, the feature points in qualified matches are used in registration for state estimation.

C. Definition of p-Index

In this section, we introduce the metric, p-Index, to measure the persistence level of a feature point in the local feature map, which is weighed by how frequent the feature point has been detected in the recent frames.

In specific, we use $\mathbf{p}_{k_0}^M$ to denote a feature point in the k_0th frame of the local feature map, i.e., $\mathbf{p}_{k_0}^M \in \mathcal{M}_{k_0}$, where k_0 is the time when the point $\mathbf{p}_{k_0}^M$ is first introduced in the local feature map. Then, for $k \geq k_0$, we define

$$\mathbf{I}(\mathbf{p}_{k_0}^M, k) = \begin{cases} 1 & \exists \mathbf{p}_k \in \mathcal{E}_k \cup \mathcal{S}_k, s.t.\ \mathbf{p}_{k_0}^M \in \mathcal{N}_k(\mathbf{p}_k), \\ 0 & \text{otherwise,} \end{cases}$$

where $\mathcal{E}_k$ and $\mathcal{S}_k$ denote the sets of extracted edge features and surface features from the kth frame of LiDAR data, respectively. $\mathcal{N}_k(\mathbf{p}_k)$ denotes the set of corresponding points in $\mathcal{M}_k$ for $\mathbf{p}_k$ from a resulting match after the rough filter process. Intuitively, $\mathbf{I}(\mathbf{p}_{k_0}^M, k) = 1$ indicates that there exists an extracted feature point in the kth frame that can be matched with the point $\mathbf{p}_{k_0}^M$. In the following, a feature point $\mathbf{p}_{k_0}^M$ is called to be *detected* in the kth frame, if $\mathbf{I}(\mathbf{p}_{k_0}^M, k) = 1$.
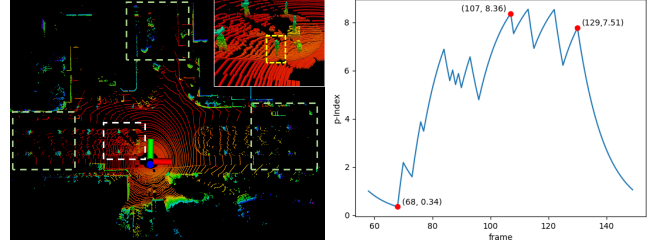
Similar to the eligibility traces approach [26], we use p-Index to specify how frequency and recency of a feature point that can be detected in past consecutive frames. In particle, p-Index of a feature point $\mathbf{p}_{k_0}^M$ in the kth frame ($k \geq k_0$) is defined as:

$$\text{p-Index}(\mathbf{p}_{k_0}^M, k_0) = \gamma\,\mathbf{I}(\mathbf{p}_{k_0}^M, k_0),$$
$$\text{p-Index}(\mathbf{p}_{k_0}^M, k) = \gamma\,(\text{p-Index}(\mathbf{p}_{k_0}^M, k-1) + \mathbf{I}(\mathbf{p}_{k_0}^M, k)),$$

for some $\gamma \in [0, 1]$. Note that, the above recursive equations are algebraically equivalent to the following formula:

$$\text{p-Index}(\mathbf{p}_{k_0}^M, k) = \sum_{\tau=k_0}^{k} \gamma^{k+1-\tau}\mathbf{I}(\mathbf{p}_{k_0}^M, \tau). \quad (3)$$

Intuitively, a larger value of p-Index is assigned to those feature points that have been detected more frequently recently. In Eq. (3), γ specifies the effect of the time interval on the value of p-Index. The reason for introducing γ is

(a) The point cloud at the 100-th frame. The green dotted box indicates a sparse point cloud and the detail in the white dotted box is shown in the top right.

(b) The values of p-Index w.r.t. consecutive frames for an edge feature point.

Fig. 3. Illustration of the p-Index value. (b) illustrates the values of p-Index for an an edge feature on a pole inside the yellow dotted box in (a). At the 58th frame, it first appears in the LiDAR's FOV. It is continuously detected from the 68th frame to the 107th frame. Finally, only few (about three) points on the pole are scanned at the 129th frame; afterwards this edge feature is no longer detected.

that the point cloud is densely distributed nearby the agent and sparsely distributed in the distance, as illustrated in Fig. 3. When the agent is moving forward, k increases and landmarks near the agent at the τth ($\tau \leq k$) frame will be left behind. Then the point cloud at the kth frame around the landmark would be distributed sparsely, where the corresponding feature points would no longer be important. In particular, when $k + 1 - \tau$ increases, $\gamma^{k+1-\tau}$ would converge to 0, which reduces the weight of $\mathbf{I}(\mathbf{p}_{k_0}^M, \tau)$ in p-Index$(\mathbf{p}_{k_0}^M, k)$.

We set θ_p as the threshold to identify persistent feature points. In specific, a feature point $\mathbf{p}_{k_0}^M$ is *persistent* at the kth frame, if p-Index$(\mathbf{p}_{k_0}^M, k) > \theta_p$. Otherwise, $\mathbf{p}_{k_0}^M$ is *transient*. Note that, the larger the θ_p, the fewer the persistent feature points.

D. Building Persistent Maps through PFilter

Now we specify details of our feature filtering algorithm, *PFilter*. In specific, at the kth frame, we first update p-Index$(\mathbf{p}_{k_0}^M, k)$ for each feature point $\mathbf{p}_{k_0}^M$ in the local feature map. We also estimate an initial value of p-Index$(\mathbf{p}_k, k)$ for each feature point $\mathbf{p}_k \in \mathcal{E}_k \cup \mathcal{S}_k$, i.e., extracted feature points from LiDAR data, using the average value of p-Index for five feature points that correspond to $\mathbf{p}_k$ in the match. Then we add these extracted feature points with their initial values of p-Index to the local feature map. For each feature point $\mathbf{p}_{k_0}^M$ in the local feature map, if $\mathbf{p}_{k_0}^M$ has just been detected recently, i.e., $k - k_0 < \kappa_{new}$ for a small natural number κ_{new}, then we maintain it in the local feature map for a while to see whether it would be persistent or not. If p-Index of $\mathbf{p}_{k_0}^M$ is larger than a constant θ_{max}, i.e., p-Index$(\mathbf{p}_{k_0}^M, k) > \theta_{max} \in [\gamma, \frac{\gamma}{1-\gamma})$, then this feature point will be maintained in the local feature map permanently. At last, we remove the feature point from the local feature map, if p-Index$(\mathbf{p}_{k_0}^M, k) \leq \theta_p$.

The process of *PFilter* is summarized in Alg. 1.

- The input involves a local edge map, denoted as $\mathcal{M}_k^e$, a local surface map, denoted as $\mathcal{M}_k^s$, the extracted edge and surface features, denoted as $\mathcal{E}_k$ and $\mathcal{S}_k$, and the optimal pose, denoted as $\mathbf{T}_k^{k+1}$.

Algorithm 1: *PFilter*

Data: $\mathcal{M}_k^e$, $\mathcal{M}_k^s$, $\mathcal{E}_k$, $\mathcal{S}_k$, $\mathbf{T}_k^{k+1}$
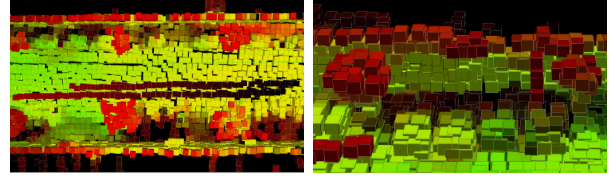**Result:** $\mathcal{M}_{k+1}^e$, $\mathcal{M}_{k+1}^s$

1 **for** e_k **in** $\mathcal{E}_k$ **do**
2     $\mathbf{e}_k \leftarrow \mathbf{T}_k^{k+1}\mathbf{e}_k$;
3     $\mathcal{N}_k(\mathbf{e}_k) \leftarrow$ Find_correspondence$(\mathbf{e}_k, \mathcal{M}_k^e, 5)$;
4   **for** $\boldsymbol{p}_{k_0}$ **in** $\mathcal{N}_k(\boldsymbol{e}_k)$ **do**
5   p-Index$(\mathbf{p}_{k_0}, k) \leftarrow$ p-Index$(\mathbf{p}_{k_0}, k) + 1$;
6   **end**
7   p-Index$(\mathbf{e}_k, k) =$ Average(p-Index$(\mathbf{p}_{k_0}, k)$ **for** $\mathbf{p}_{k_0}$ **in** $\mathcal{N}_k(\mathbf{e}_k)$);
8 **end**
9 $\mathcal{M}_{k+1}^e \leftarrow \mathcal{M}_k^e \cup \mathcal{E}_k$;
10 **for** $\boldsymbol{p}_{k_0}$ **in** $\mathcal{M}_{k+1}^e$ **do**
11   **if** p-Index$(\boldsymbol{p}_{k_0}, k) > \theta_p$ **then**
12   **if** p-Index$(\mathbf{p}_{k_0}, k) \geq \theta_{max}$ **then**
13   p-Index$(\mathbf{p}_{k_0}, k) \leftarrow +\infty$
14   **end**
15   p-Index$(\mathbf{p}_{k_0}, k+1) \leftarrow \gamma \cdot$p-Index$(\mathbf{p}_{k_0}, k)$;
16   continue;
17   **else if** $k - k_0 < \kappa_{new}$ **then**
18   p-Index$(\mathbf{p}_{k_0}, k+1) \leftarrow \gamma \cdot$p-Index$(\mathbf{p}_{k_0}, k)$;
19   continue;
20   **end**
21   Delete$(\mathbf{p}_{k_0})$;
22 **end**
23 Compute $\mathcal{M}_{k+1}^s$ w.r.t. $\mathcal{S}_k$, $\mathcal{M}_k^s$ following the similar procedure.

- Lines 1-7: The loop intends to estimate the value of p-Index for each extracted feature point in $\mathcal{E}_k$ (resp. $\mathcal{S}_k$). Meanwhile, p-Index for each feature point in the local feature map is also updated in Line 4-6.
- Line 9: Extracted feature points with their initial values of p-Index are introduced to the local feature map.
- Lines 10-22: The loop intends to remove feature points from the local feature map, if their values of p-Index are lower than θ_p. Meanwhile, we reserve points that are recently detected or whose values of p-Index are used to be larger than θ_{max}. For the transient feature points, we remove them in line 21.

Notice that, *PFilter* can significantly reduce the number of feature points in the local feature map. This can also reduce the computational cost for identifying legal matches in the rough filter process, as there would be fewer corresponding points in the local feature map that need to be considered for an extracted feature point from LiDAR data.

V. EXPERIMENTS

We implement our feature filtering algorithm *PFilter* and integrate it into the well-established scan-to-map LiDAR odometry framework, F-LOAM. We first evaluate the performance of the improved LO system on the KITTI dataset. The experimental results show that *PFilter* can improve both accuracy and efficiency of F-LOAM. Later, we show

(a) The trajectories of moving pedestrians   (b) The mistakenly extracted surface feature points

Fig. 4. The local surface feature map for an environment in KITTI. The color of the feature points from green to red indicates the value of p-Index from high to low. The trajectories of moving pedestrians are indicated by the red-black lines in (a). (b) shows a detail of the environment involving the surface feature points correspond to static landmarks, but were extracted incorrectly. These transient feature points are identified by p-Index automatically.

that persistent feature points usually correspond to static landmarks and transient feature points usually correspond to moving objects or noise in various typical environments. Then, we construct an ablation study to examine the effects of values of corresponding parameters, i.e., θ_p, θ_{max}, and κ_{new}. At last, we compare the performance of *PFilter* based on two feature extraction methods in Sec. III-B, respectively. The result shows that, *PFilter* is not sensitive to specific feature extraction methods.

All experiments are conducted on a laptop with an AMD Ryzen 7 4800H CPU and 16GB memory. The parameter γ in Eq. (3) is set to be 0.6.

A. Performance on KITTI

KITTI [15] odometry benchmark is one of the most popular datasets for evaluating visual or LiDAR-based SLAM. The LiDAR used in the dataset is Velodyne HDL-64E, and the ground truth is given by the output of the GPS/IMU localization unit. It provides 11 sequences with ground truth that contains urban, country, and highway scenes. In our experiment, we set $\theta_p = 1.5$, $\theta_{max} = 2$, and $\kappa_{new} = 2$.

Table. I summarizes the accuracy of F-LOAM integrated with *PFilter*, as well as a few other LO systems. We use average translational error, ATE (m/100m), as in [15] to evaluate the accuracy of LO systems. We compare our improved F-LOAM with LOAM, A-LOAM, LeGo-LOAM, and the original version of F-LOAM.

Table. II summarizes the average number of feature points in local maps, the average number of constrains used to estimate ego-motion, and the average time spent on registration of F-LOAM with or without *PFilter*. We use Δ to denote the ratio of the reduction for the above metrics. Note that 'w/' and 'w/o' mean "with" and "without" in tables.

As shown in Table. I and II, *PFilter* can significantly reduce the number of feature points for the registration process, can effectively alleviate the bottleneck, and can considerably improve the system accuracy. To be more precise, it removes about 48.4% of the points in the local feature map and reduce feature points in scan by 19.3% on average, which improves the efficiency of the SLAM system by 20.9% and improve the accuracy by 9.4%.
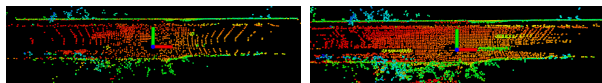
TABLE I

ATE(%) OF LO SYSTEMS ON KITTI DATASET

LO Systems	00	01	02	03	04	05	06	07	08	09	10	Mean
LOAM [8]	0.78	**1.43**	**0.92**	**0.86**	0.71	0.57	0.65	0.63	1.12	0.77	**0.79**	**0.84**
A-LOAM	**0.69**	1.96	4.53	0.94	0.72	0.49	0.59	0.42	1.04	0.73	1.00	1.19
LeGO-LOAM [16]	1.38	28.03	2.14	1.21	1.27	0.91	0.80	0.74	1.40	1.25	1.70	3.71
F-LOAM [9]	0.70	1.95	1.04	0.95	**0.68**	**0.49**	**0.54**	**0.42**	**0.93**	**0.70**	1.02	0.85
F-LOAM with *PFilter*	**0.61**	**1.77**	**0.80**	**0.89**	**0.65**	**0.51**	**0.47**	**0.38**	**0.91**	**0.62**	**0.88**	**0.77**

Red and **blue** indicate the first and second best results respectively.

TABLE II

COMPARED WITH F-LOAM

seq	Number of feature points in local feature map			Number of constrains			Time(ms)		
	F-LOAM	F-LOAM w/ *PFilter*	$\Delta(\%)$	F-LOAM	F-LOAM w/ *PFilter*	$\Delta(\%)$	F-LOAM	F-LOAM w/ *PFilter*	$\Delta(\%)$
00	90,465	50,345	44.3	2,758	2,340	15.1	54.1	43.1	20.3
01	84,775	30,273	64.3	4,127	2,538	38.5	68.8	51.1	25.7
02	72,660	42,494	41.5	2,946	2,481	15.8	52.6	42.4	19.4
03	91,788	47,109	48.7	3,927	3,083	21.5	62.9	50.0	20.5
04	78,773	33,086	58.0	3,749	2,957	21.1	63.4	49.6	21.7
05	90,940	52,487	42.3	3,056	2,557	16.3	55.3	44.6	19.3
06	90,241	44,861	50.3	4,596	3,657	20.4	66.8	53.3	20.2
07	90,062	47,752	47.0	2,770	2,378	14.2	53.3	41.7	21.8
08	109,777	56,327	48.7	3,325	2,635	20.8	63.5	47.9	24.6
09	86,714	47,100	45.7	3,384	2,757	18.5	59.0	47.1	20.2
10	74,428	43,756	41.2	2,673	2,396	10.4	49.6	41.5	16.3
Mean	87,329	45,053	48.4	3,635	2,925	19.3	59.0	46.6	20.9

(a) $\theta_p = 2, \theta_{max} = \infty, \kappa_{new} = 0.$ (b) $\theta_p = 2, \theta_{max} = \infty, \kappa_{new} = 3.$

(c) $\theta_p = 2, \theta_{max} = 2, \kappa_{new} = 0$ (d) $\theta_p = 1, \theta_{max} = \infty, \kappa_{new} = 0$

Fig. 5. The effects of θ_p, θ_{max} and κ_{new}.

B. Persistent Feature Points in a Real-world Environment

As illustrated in Fig. 4, we show how *PFilter* works in a real-world environment. The environment in Fig. 4 is a street in the KITTI 00 sequence with ground, wall, trees, and moving pedestrians. Fig. 4 shows the surface feature map for the environment, where the color of the feature points from green to red indicates the value of p-Index from high to low. Fig. 4(a) shows the trajectories of moving pedestrians which is composed of surface feature points extracted from the pedestrians at different frames. Fig. 4(b) shows detail of the surface feature map. The surface feature points correspond to static landmarks including crown of a tree, thin poles, and upper edges of walls are identified to be transient. These types of features with low p-Index are filtered by *PFilter* automatically to reduce noise in the registration process.

C. Ablation Study

We conduct an ablation study to examine the effects of values of parameters in *PFilter*, i.e., θ_p, θ_{max}, κ_{new}. We will examine the effect of one parameter by fixing other two parameters.

As shown in Fig. 5, θ_p is the threshold of p-Index that mainly controls the number of persistent points. When θ_p increases, the number of persistent feature points decreases. Note that, at the beginning, the noise is gradually filtered and the accuracy is improved. However, when θ_p exceeds a

certain threshold, the error starts to increase due to the lack of constraints.

θ_{max} and κ_{new} are designed to improve the robustness of *PFilter*. As shown in Fig. 5, θ_{max} reserve more feature points corresponding to the landmarks behind the agent. κ_{new} increase the number of feature points of where is new in FOV. Proper settings of θ_p, θ_{max} and κ_{new} can improve the performance of the system.

D. On Different Feature Extraction Methods

We have introduced two method about feature extraction in Sec. III-B, i.e., the one based on "ring" and the one based on eigenvalues. F-LOAM applies the method based on "ring". Of course, we can also replace it by the method based on eigenvalues and evaluate the performance of *PFilter* on the new system. For a fair comparison, we consider the same number of feature points extracted by both methods. Table III summarizes the performance of the resulting system with or without *PFilter*. The result shows that, *PFilter* is not sensitive to specific feature extraction methods.

VI. CONCLUSION

In this paper, we consider how to improve the efficiency and accuracy of LiDAR odometry at the same time by carefully selecting feature points for registration. We observe that a large fraction of feature points are mistakenly extracted from individual LiDAR frames due to measurement errors or motions in the environment. Further, we find that these "false" feature points can be successfully identified by examining whether they continue to be detected from a sequence of frames in the near past. By filtering out those transient feature points, we can retain those persistent ones that correspond to stationary landmarks in the environment – the true features that we should focus on in the registration.

This is one of the earliest studies that explores the distribution of feature points across a stream of frames and exploits such distributions for more efficient and accurate

TABLE III

PERFORMANCE OF *PFilter* ON TWO FEATURE EXTRACTION METHODS

seq	Based on "ring"				Based on eigenvalues			
	Number of constrains		ATE(%)		Number of constrains		ATE(%)	
	w/o *PFilter*	w/ *PFilter*	w/o *PFilter*	w/ *PFilter*	w/o *PFilter*	w/ *PFilter*	w/o *PFilter*	w/ *PFilter*
00	2,758	2,340	0.70	0.61	2,487	2,087	0.69	0.61
01	4,127	2,538	1.95	1.77	3,974	2,558	2.26	2.06
02	2,946	2,481	1.04	0.80	2,574	2,144	0.98	0.83
03	3,927	3,083	0.95	0.89	3,678	2,962	0.80	0.71
04	3,749	2,957	0.68	0.65	3,434	2,722	0.79	0.78
05	3,056	2,557	0.49	0.51	2,784	2,346	0.52	0.53
06	4,596	3,657	0.54	0.47	4,428	3,537	0.54	0.51
07	2,770	2,378	0.42	0.38	2,522	2,158	0.49	0.37
08	3,325	2,635	0.93	0.91	3,099	2,504	0.96	0.95
09	3,384	2,757	0.70	0.62	3,059	2,378	0.63	0.75
10	2,673	2,396	1.02	0.88	2,329	1,984	1.10	1.14
Mean	3,391	2,707	0.85	0.77	3,124	2,489	0.88	0.84

SLAM. Moving forward, we will examine the feature points more closely to further cut down the false ones. We will also apply such techniques on other sensors such as cameras, radars, and different types of LiDAR sensors.

ACKNOWLEDGMENT

REFERENCES

[1] C. Cadena, L. Carlone, H. Carrillo, Y. Latif, D. Scaramuzza, J. Neira, I. Reid, and J. J. Leonard, "Past, present, and future of simultaneous localization and mapping: Toward the robust-perception age," *IEEE Transactions on Robotics*, vol. 32, no. 6, pp. 1309–1332, 2016.

[2] R. Roriz, J. Cabral, and T. Gomes, "Automotive lidar technology: A survey," *IEEE Transactions on Intelligent Transportation Systems*, pp. 1–16, 2021.

[3] N. Jonnavithula, Y. Lyu, and Z. Zhang, "Lidar odometry methodologies for autonomous driving: A survey," *arXiv preprint arXiv:2109.06120*, 2021.

[4] D. Rozenberszki and A. L. Majdik, "Lol: Lidar-only odometry and localization in 3d point cloud maps*," in *2020 IEEE International Conference on Robotics and Automation (ICRA)*, 2020, pp. 4379–4385.

[5] P. J. Besl and N. D. McKay, "Method for registration of 3-d shapes," in *Sensor fusion IV: control paradigms and data structures*, vol. 1611. Spie, 1992, pp. 586–606.

[6] P. Biber and W. Strasser, "The normal distributions transform: a new approach to laser scan matching," in *Proceedings 2003 IEEE/RSJ International Conference on Intelligent Robots and Systems (IROS 2003) (Cat. No.03CH37453)*, vol. 3, 2003, pp. 2743–2748 vol.3.

[7] X. Huang, G. Mei, J. Zhang, and R. Abbas, "A comprehensive survey on point cloud registration," *arXiv preprint arXiv:2103.02690*, 2021.

[8] J. Zhang and S. Singh, "Loam: Lidar odometry and mapping in real-time." in *Robotics: Science and Systems*, vol. 2, no. 9, 2014.

[9] H. Wang, C. Wang, C. Chen, and L. Xie, "F-loam : Fast lidar odometry and mapping," in *2021 IEEE/RSJ International Conference on Intelligent Robots and Systems (IROS)*, 2020.

[10] Y. Pan, P. Xiao, Y. He, Z. Shao, and Z. Li, "Mulls: Versatile lidar slam via multi-metric linear least square," in *2021 IEEE International Conference on Robotics and Automation (ICRA)*. IEEE, 2021, pp. 11 633–11 640.

[11] J. Jiao, Y. Zhu, H. Ye, H. Huang, P. Yun, L. Jiang, L. Wang, and M. Liu, "Greedy-based feature selection for efficient lidar slam," in *2021 IEEE International Conference on Robotics and Automation (ICRA)*. IEEE, 2021, pp. 5222–5228.

[12] W. Li, Y. Hu, Y. Han, and X. Li, "Kfs-lio: Key-feature selection for lightweight lidar inertial odometry," in *2021 IEEE International Conference on Robotics and Automation (ICRA)*. IEEE, 2021, pp. 5042–5048.

[13] Z. Wan, Y. Zhang, B. He, Z. Cui, W. Dai, L. Zhou, and G. Huang, "Observation contribution theory for pose estimation accuracy," *arXiv preprint arXiv:2111.07723*, 2021.

[14] J. Wang, M. Xu, F. Foroughi, D. Dai, and Z. Chen, "Faster-gicp: Acceptance-rejection sampling based 3d lidar odometry," *IEEE Robotics and Automation Letters*, vol. 7, no. 1, pp. 255–262, 2021.

[15] A. Geiger, P. Lenz, and R. Urtasun, "Are we ready for autonomous driving? the kitti vision benchmark suite," in *Conference on Computer Vision and Pattern Recognition (CVPR)*, 2012.

[16] T. Shan and B. Englot, "Lego-loam: Lightweight and ground-optimized lidar odometry and mapping on variable terrain," in *2018 IEEE/RSJ International Conference on Intelligent Robots and Systems (IROS)*, 2018, pp. 4758–4765.

[17] K. Li, M. Li, and U. D. Hanebeck, "Towards high-performance solid-state-lidar-inertial odometry and mapping," *IEEE Robotics and Automation Letters*, vol. 6, no. 3, pp. 5167–5174, 2021.

[18] J. Lin and F. Zhang, "Loam livox: A fast, robust, high-precision lidar odometry and mapping package for lidars of small fov," in *2020 IEEE International Conference on Robotics and Automation (ICRA)*. IEEE, 2020, pp. 3126–3131.

[19] Z. Zhou, M. Yang, C. Wang, and B. Wang, "Roi-cloud: A key region extraction method for lidar odometry and localization," in *2020 IEEE International Conference on Robotics and Automation (ICRA)*. IEEE, 2020, pp. 3312–3318.

[20] H. Yin, Y. Wang, L. Tang, X. Ding, S. Huang, and R. Xiong, "3d lidar map compression for efficient localization on resource constrained vehicles," *IEEE Transactions on Intelligent Transportation Systems*, vol. 22, no. 2, pp. 837–852, 2020.

[21] F. Pomerleau, P. Krüsi, F. Colas, P. Furgale, and R. Siegwart, "Long-term 3d map maintenance in dynamic environments," in *2014 IEEE International Conference on Robotics and Automation (ICRA)*. IEEE, 2014, pp. 3712–3719.

[22] H. Dong, X. Chen, and C. Stachniss, "Online range image-based pole extractor for long-term lidar localization in urban environments," in *2021 European Conference on Mobile Robots (ECMR)*, 2021, pp. 1–6.

[23] Y. He, L. Ma, Z. Jiang, Y. Tang, and G. Xing, *VI-Eye: Semantic-Based 3D Point Cloud Registration for Infrastructure-Assisted Autonomous Driving*. New York, NY, USA: Association for Computing Machinery, 2021, p. 573–586. [Online]. Available: https://doi.org/10.1145/3447993.3483276

[24] W. Hess, D. Kohler, H. Rapp, and D. Andor, "Real-time loop closure in 2d lidar slam," in *2016 IEEE International Conference on Robotics and Automation (ICRA)*, 2016, pp. 1271–1278.

[25] J.-E. Deschaud, "Imls-slam: Scan-to-model matching based on 3d data," in *2018 IEEE International Conference on Robotics and Automation (ICRA)*. IEEE, 2018, pp. 2480–2485.

[26] R. S. Sutton and A. G. Barto, *Reinforcement learning: An introduction*. MIT press, 2018.